INDIAN JOURNAL OF SCIENCE AND TECHNOLOGY

RESEARCH ARTICLE

Numerical Analysis of the Influence of an Inclined Magnetic Field on the Flow of Casson Nanofluid Across an Exponentially Stretching Surfae, using the Darcy-Forchheimer model

Rekha Devi[1]*, **Shilpa Sood**[2]

1 Research Scholar , Department of Mathematics and Statistics, Career Point University, Hamirpur, Himachal Pradesh, India
2 Associate Professor, Department of Mathematics and Statistics , Career Point University, Hamirpur, Himachal Pradesh, India

OPEN ACCESS

Received: 01-10-2023
Accepted: 11-10-2023
Published: 28-11-2023

Citation: Devi R, Sood S (2023) Numerical Analysis of the Influence of an Inclined Magnetic Field on the Flow of Casson Nanofluid Across an Exponentially Stretching Surfae, using the Darcy-Forchheimer model. Indian Journal of Science and Technology 16(44): 4081-4089. https://doi.org/10.17485/IJST/v16i44.2481

* **Corresponding author**.

rekha111179@gmail.com

Funding: None

Competing Interests: None

Published By Indian Society for Education and Environment (iSee)

ISSN
Print: 0974-6846
Electronic: 0974-5645

Abstract

Objective: The present study analyses the heat transfer properties of a Casson fluid moving under the influence of an inclined magnetic field through an exponentially stretched surface in a porous medium using the Darcy-Forchheimer law. Non-Newtonian fluid behavior is described by using the Casson fluid model. Thermophoresis as well as Brownian motion effects on heat transmission and concentration of nanoparticle are considered. **Method:** With similarity transformations; nonlinear (PDE) partial differential equation has been changed to (ODEs) ordinary differential equations. By using bvp4c programme in the Matlab software, the nonlinear PDE are numerically solved. **Findings:** The impacts of dimensionless factors on the flow, concentration of nanoparticle and heat transfer were studied. Graphs were plotted and analyzed in order to explore how different dimensionless factors affected velocity, temperature concentration profiles. **Novelty:** The combination of magnetic fields, nanofluids, and the Darcy-Forchheimer model is an interdisciplinary approach. Future researchers in fields like fluid dynamics, magneto hydrodynamics, materials science, and applied mathematics could benefit from this research work. It bridges multiple disciplines and contributes to the ongoing efforts to make energy-related processes more efficient and sustainable. The findings demonstrate that the porous medium is accountable for both inflation in the thermal boundary layer thickness and a decrease in the thickness of the momentum boundary layer. For increasing the permeability of the medium, conductive heat transfer predominates. The improvement of heat and mass transport is made possible by all these elements.

Keywords: Casson fluid; Heat transmission; Nonlinear PDE.; Darcy-Forchheimer law; Porous medium

1 Introduction

The investigation on the effects of heat transfer and mass on MHD flow has garnered considerable attention in research due to its relevance to various industrial and engineering applications. These applications span a wide range and include areas such as geothermal energy extraction, nuclear reactors, plasma studies, and MHD generators. Researchers have focused on studying the behavior of electrically conducting, viscous, and incompressible fluids in order to better understand and optimize these processes. Both the polymer and biomechanics industries depend significantly on casson fluids.

The scientific literature is full with numerical and experimental analyses on the improved thermal properties with nanofluid. Thermal performance can be actively improved as a result of heat transfer and mass effects brought about by magneto hydrodynamic (MHD) nanofluid flowing through a porous medium by using Darcy–Forchheimer Flow across an Inclined Sheet[1]. Sharma[2] explored the Williamson nanofluid flow in the MHD boundary layer by employing a curved stretching sheet. Arifuzzaman et al.[3] determined $Al_2O_3 - H_2O$ nanofluid within a square vessel while being subjected to a MHD field and an exothermic chemical reaction.

Uddin et al. conducted computational research on the natural convection transfer of heat of a CuO –H_2O nanofluid contained inside a quadrilateral vessel[4]. Irfan et al. found a heat sink and/or source along with chemical reaction in the Maxwell nanofluid stagnation point flow[5]. In the radiative Maxwell nanofluid flow, Rafiq et al.presented the Arrhenius activation energy theory[6]. Irfan investigated thermophoretic diffusion and Brownian motion in a nonlinear Carreau nanofluid mixed convection flow with changing characteristics[7]. In many technological and industrial processes, porous media effectively handle the transmission of fluid velocity and heat. For the flow through a porous media, Darcy[8] provided a classical theory. But this theory holds true for analysis with lower velocity and less porosity. Conversely, the classical Darcy theory is invalidated and expanded when a fluid is moving at a higher velocity. The flow of fluid is modeled using the Darcy-Forchheimer equation[9]. The past mentioned findings and their analysis uses in engineering, geophysics, aerodynamics, biological sciences, as well as industrial sectors served as the inspiration for this study. Waini et al.[10]flow and heat transfer over a moving thin needle. MHD Stagnation-point flow and transfer of heat in a micropolar fluid over an exponentially sheet. The prior literature makes it quite evident that no one has considered such kinds of flow situations. The outcomes are provided with bvp4c solver. The research conducted by Recently, Sharma and Sood[11] studied inclined magnetic field on flow of Williamson nanofluid in Darcy-Forchheimer Model.

We concentrate on the heat transfer and flow of a casson fluid boundary layer over an exponentially stretched sheet in current study. Numerous dimensionless parameter values for the issue were computed numerically, to the acceptable level of precision. The results were thoroughly discussed. Several factors considerably impact the heat transfer and field flow when injection or suction is present at the wall. Additionally taken into consideration is the assessment of skin friction, which is crucial in terms of industrial applications. The impacts of various significant factors on the characteristics of mass transfer, heat, and momentum were investigated, and the numerical outcomes are displayed graphically and in the form of tabular. Inspired by the aforementioned discoveries and their growing research applications in geophysics, engineering, biological sciences, aerodynamics, and industrial industries, the basic objective of the present work is to explore the impact of two-dimensional MHD boundary layer flow of casson nanofluid over an exponentially stretching sheet under the effects of an inclined magnetic field, using the Darcy-Forchheimer model. It is clear from the previous literature that no one has thought about these types of flow circumstances in casson nanofluid.

2 Methodology

In this study, we have considered casson nano fluid 2D- magnetohydrodynamic boundary layer flow over a sheet that is exponentially stretched within a porous medium. We consider that the surface have a constant temperature T_w and that the fraction of nanofluid volume C_w . The volume and temperature fraction of in viscid $T_\infty C_\infty$. Furthermore, in scenario, $U_w(x) = U_0 e^{x/L}$. The momentum equation includes the Forchheimer quadratic drag term, and it is assumed that the flow rate is very high. A magnetic field that is inclined is also imposed parallel to the surface. Mustafa and Eldabe provide the equation of state for the casson fluid in an isotropic flow, reads as[12,13] :

$$\tau_{ij} = \begin{pmatrix} \left((2\mu_B + \frac{\tau_y}{\sqrt{2\Pi}})\right) e_{ij}, \ for\ \pi \geq \pi_c, , \\ \left(2\mu_B + \frac{\tau_y}{\sqrt{2\Pi}})\right) e_{ij}, \ for\ \pi \leq \pi_c, \end{pmatrix}$$

Here, deformation rate of component is $\pi = e_{ijj}\, e_{ij}$ when it is compared to itself with (i, j), π_c indicates component of the rate of deformation is considered to be the important product value resulting from the non-Newtonian model. τ_y as well as μ_B indicate fluid yield stress and fluid plastic dynamic viscosity, respectively. The governing equations for energy, momentum, continuity,

and concentration in this type of flow are expressed as follows:[12,14].

$$\frac{\partial U*}{\partial x}+\frac{\partial V*}{\partial y}=0 \tag{1}$$

$$U*\frac{\partial U*}{\partial x}+V*\frac{\partial U*}{\partial y}=(1+\frac{1}{\beta})\nu\frac{\partial^2 U*}{\partial y^2}-FU*^2-\frac{B^2}{\rho}U*sin^2(\alpha)-\frac{\nu}{K}U* \tag{2}$$

$$U*\frac{\partial T}{\partial x}+V*\frac{\partial T}{\partial y}=\gamma\frac{\partial^2 T}{\partial y^2}+\frac{\rho_p C_p}{\rho C}\left[D_B*\frac{\partial C*}{\partial y}\frac{\partial T}{\partial y}+\frac{D_T}{T_\infty}\left(\frac{\partial T}{\partial y}\right)^2\right] \tag{3}$$

$$U*\frac{\partial C*}{\partial x}+V*\frac{\partial C*}{\partial y}=\frac{D_T}{T_\infty}\frac{\partial^2 T}{\partial y^2}+\frac{\partial^2 C*}{\partial y^2}D_B* \tag{4}$$

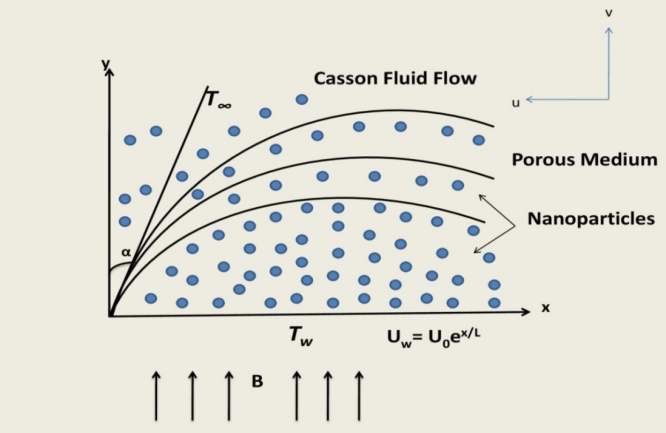

Fig 1. Physical configuration of the study

The following boundary conditions have been defined for the study:

$$U*=U_w=U_0e^{\frac{x}{L}},V*=0,C*=C_wT=T_w\ at\ Y=0,$$

$$U*=0,V*=0,C*\to C_\infty,T\to T_\infty\ as\ Y\to\infty \tag{5}$$

2.1 Similarity transformations

The boundary conditions as well as nonlinear partial differential equations (1-5) have been transformed to ODEs using similarity transformations.

$$\psi=(2\nu LU_0)^{\frac{1}{2}}G(\eta)e^{\frac{x}{2L}},\eta=Y\sqrt{(\frac{U_0}{2\nu L})}e^{\frac{X}{2L}},U*=U_0e^{\frac{x}{L}},V*=-[G(\eta)+\eta G'(\eta)]\sqrt{(\frac{\nu U_0}{2L})}e^{\frac{X}{2L}},$$

$$T=T_0e^{\frac{X}{2L}}\theta(\eta)+T_\infty,C*=C_0e^{\frac{x}{2L}}+C_\infty$$

By adding the stream function ψ so that $V*=-\frac{\partial\psi}{\partial x}$ as well as $U*=\frac{\partial\psi}{\partial y}$ represents functions of η. The transformed ordinary equations (6-9) are as follows after applying the similarity transformations:

$$G'''(1+\frac{1}{\beta})+GG''-(K_p+Msin^2(\alpha))G'-(2+Fr)G''=0 \tag{6}$$

$$\theta'''+(G\theta'+N_t\theta''-G'\theta+N_b\theta'\phi')\Pr=0 \tag{7}$$

$$\phi'' - Le(G'\phi - G\phi') + \theta'' \frac{N_t}{N_b} = 0 \tag{8}$$

$$G(0) = 0, G'(0) = 1, \theta(0) = 1, \phi(0) = 1 \quad at \quad \eta \to 0. \tag{9}$$

$$G'(\infty) = 0, \theta(\infty) = 0, \phi(\infty) = 0 \text{ at } \eta \to \infty$$

The dimensionless parameters are provided as follows:

$$Fr = \frac{C_b}{2\sqrt{k*}}, M = \frac{2\sigma B^2 L}{\rho U_w}, K_p = \frac{2\nu L}{K U_w}, \beta = \frac{\mu_{\beta\sqrt{2\pi}}}{\tau_y} \Pr = \frac{\nu}{\gamma}, N_b = \frac{D_B (C_w - C_\infty)(\rho C)_p}{\nu(\rho C)_f}$$

Here Fr indicates Forchheimer number, M is magnetic field parameter, K_p defines porosity parameter, β shows casson fluid parameter, Pr defines Prandtl number, N_b expresses diffusivity parameter, N_t defines thermophoresis parameter. The local Nusselt number, skin friction coefficient, and Sherwood number are defined as follows:

$Nu_X = \frac{xq_{w\circ}}{\kappa(T_w - T_\infty)}, C_{fX} = \frac{\tau_{w\circ}}{\rho U_w{}^2(x)}, Sh_x = \frac{xq_{m\circ}}{D_B*(C_w - C_\infty)}$

Here casson nano fluid shear stress at the wall's surface is calculated $\tau_{w\circ}$ $q_{m\circ}$ as well as $q_{w\circ}$ provide them as sand heat fluxes from the wall, respectively. These are the terms listed as

$$\tau_{w\circ} = \mu_0 \left(1 + \frac{1}{\beta}\right) \frac{\partial^2 U*}{\partial y^2}, q_{w\circ} = -\varsigma \left(\frac{\partial T}{\partial y}\right)_{y=0}, \; q_{m\circ} = -D_B * \left(\frac{\partial C*}{\partial y}\right)_{y=0}.$$

The non-dimensional forms of the parameters mentioned can be defined by applying similarity transformations as well as dominated boundary conditions.

$$C_{fx}(Re)^{\frac{1}{2}} = \left(1 + \frac{1}{\beta})G''(0)\right)$$

$$Nu_x(Re)^{-\frac{1}{2}} = \left(-\theta'(\eta)\right) \; at \; \eta = 0$$

$$Sh_x(Re)^{-\frac{1}{2}} = \left(-\phi'(\eta)\right) \; at \; \eta = 0$$

2.2 Implementation of the bvp4c Solver

This research has discussed a bvp4c explanatory implementation for the study under consideration. By using similarity transformations, we convert PDEs into ODEs. The process demonstration was provided by Shampine[15]. Using bvp4c Solver, we get equations (10)-(15)

Step-1

$$G = \Lambda(1), G' = \Lambda(2), G'' = \Lambda(3), \theta = \Lambda(4), \theta' = \Lambda(5), \phi = \Lambda(6), \phi' = \Lambda(7) \tag{10}$$

Step-2

$$G' = \Lambda(2), G'' = \Lambda(3) \tag{11}$$

$$G''' = -\Lambda(1)\Lambda(3) + \left(K_p + M\sin^2(\alpha)\right)\Lambda(2) + (2 + Fr)\Lambda(3) / \left(1 + \frac{1}{\beta}\right) \tag{12}$$

$$\theta'' = -\Pr\Lambda(1)\Lambda(5) - \Lambda(2)\Lambda(4) + (Nb)\Lambda(5)\Lambda(7) + (Nt)\Lambda(5)^2) \tag{13}$$

$$\phi'' = -Le\Lambda(1)\Lambda(7) - \Lambda(2)\Lambda(6)) + (Nt/Nb)\Pr(\Lambda(1)\Lambda(5)) - \Lambda(2)\Lambda(4) + (Nb)\Lambda(5)\Lambda(7) + (Nt)\Lambda(5)^2] \tag{14}$$

Step-3

The boundary conditions change as a consequence of new variables:

$$\Lambda_a(1) = 0, \Lambda_a(2) = 1, \Lambda_a(4) = 1, \Lambda_a(6) = 1, \Lambda_b(2) = 0, \Lambda_b(4) = 0, \Lambda_b(6) = 0 \tag{15}$$

The position at is described by Λ_a at $\eta = 0$ whereas as $\eta \to \infty$ is described by Λ_b

Step-4

The bvp4c solver in MATLAB is utilized for solving a system of first-order equations with boundary conditions. To maintain accuracy, initial assumptions, boundary layer edge position, and step size are changed as necessary.

3 Result and Discussion

In our study, we have investigated heat transfer and the impacts of many increase in physical parameters including K_p, Le, Pr, N_b, N_t, Fr and β on temperature θ (η),velocity $G'(\eta)$, as well as nanoparticle concentration profiles $\phi(\eta)$ and the findings were shown by figures. With a few previously published studies, we have compared our results to make sure our assumptions are reasonable and our code is reliable. A comparison of θ' (0) values for various Pr values in Table 1 in such a way that $K_p = \alpha = N_t = 0 = Fr = M = Le$. We noticed that good agreement between the obtained findings with the findings of Magyari & Sharma & Sood [11], Keller [16], and Sharma [17].

Table 1. Comparative - $\theta'(0)$ values for distinct Pr values

M	Pr	Magyari & Keller	Sharma & Sood	Sharma	Present study
0	1	0.954782	0.9548	0.9548	0.9507
0	2	1.4714	1.4715	—–	1,4724
0	3	1.869075	1.8690	1.8691	1.8652
0	5	—–	2.5001	2.5001	2.4997
0	10	3.660379	3.6603	0.9548	3.6537
1	1	—	0.8615	0.8611	0.8616

Figures 2, 3 and 4 respectively, show graphical representations of velocity profiles against Fr, α and β. The inverse relation between the porous medium permeability and the Forchheimer parameter, as can be seen in Figure 1. Plorification in Fr results in a drop in the medium permeability and, therefore, a reduction in cross-sectional area, which causes a decline in velocity profiles. Figure 3 clearly demonstrates that an inclined angle α leads to a declining trend in the velocity distribution. The non-Newtonian properties of the Casson fluid are shown in Figure 4. The aforementioned fluid becomes more viscous as forces grow. This occurs because, when casson parameter increases, relaxation time also increases flow resistance. Therefore, viscous forces dominate fluid motion more strongly and velocity decreases. As the Casson parameter value increased, the results of the research showed that there was a decline in velocity. Furthermore, the value of β rises which causes the thickness of the momentum layer to decrease. However, the temperature and concentration profiles show a decline with rising Forchheimer parameter. It is clear from Figures 6, 7, 8 and 9 that the magnetic factors affect temperature and velocity profiles, respectively. As M increases, both of these profiles enhance. Because the nanoparticles act as energy carriers, this happens when the fluid's temperature rises. Additionally, because the density of nanofluid and magnetic parameter are inversely related, rising M causes the density to drops, which elevates the temperature profile. Higher value of Brownian diffusion and thermophoresis result in increased random mobility of nanoparticles in the base fluid. Conversely, concentration profiles decrease as N_b rises. As the Lewis number increases, the fluid tends to have lower nanoparticle diffusivity and a higher viscosity. As a result, as temperatures increase under the influence of Le and concentration profiles fall.

The above table shows an extensive overview of the alterations in skin friction, Nusselt number and Sherwood number are displayed through Table 2. With enhancing values of Kp, M, Fr, and α and reducing with λ, Skin friction coefficient is increasing parameters. Local Nusselt number is drops with rising values of Kp, M, Fr, λ, and α. On the other hand, local Sherwood number also decelerates with Kp, M, Fr, while the reverse trend has been noticed in the behavior of λ and α.

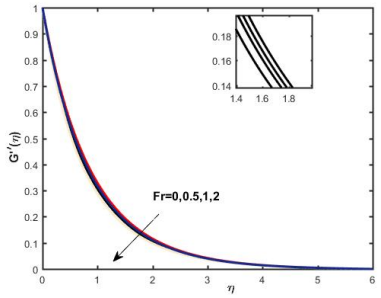

Fig 2. Impact of distinct values of Fr on velocity profiles

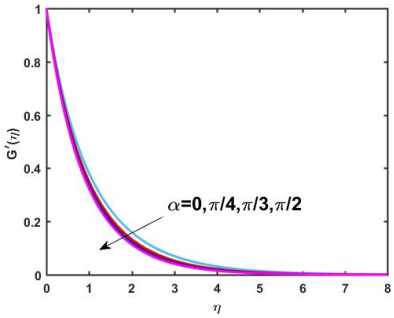

Fig 3. Impact of distinct values of α on velocity profiles

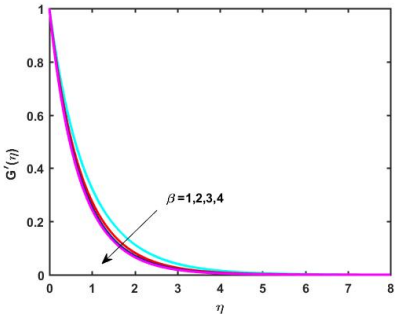

Fig 4. Impact of distinct values of β on velocity profiles

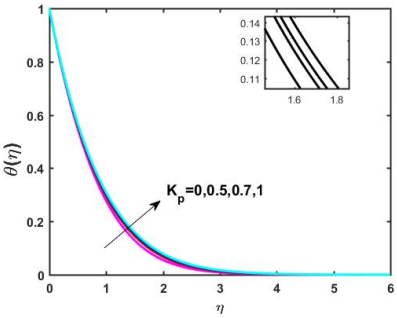

Fig 5. Impact of different values of K_p

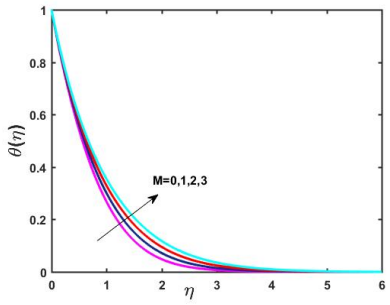

Fig 6. Impact of different values of M on temperature profiles

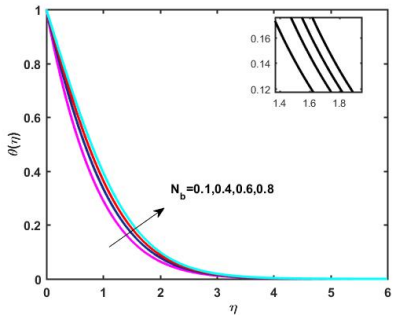

Fig 7. Impact of different values of N_b on temperature profiles

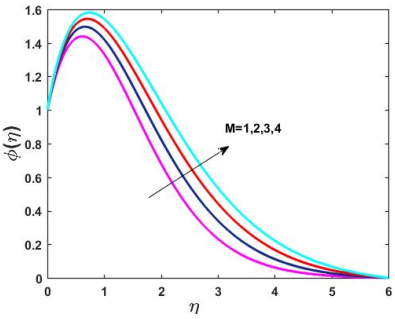

Fig 8. Impact of different values of M on concentration profiles

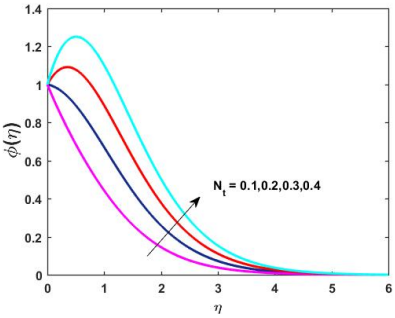

Fig 9. Impact of different values of N_t on concentration profiles

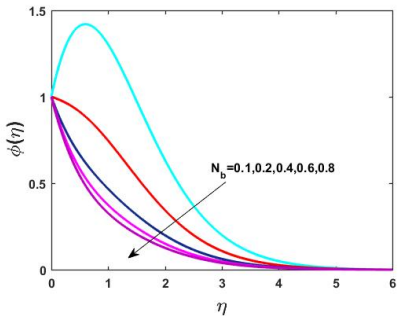

Fig 10. Impact of different values of N_b on concentration profiles

Table 2. Numerical outcomes for distinct values of significant parameters for the C_{fx} (Re) $^{1/2}$, $Nu_x(\mathrm{Re})^{-1/2}$, Sh_x (Re)$^{-1/2}$

Kp	M	Fr	β	α	Pr	$C_{fx}(\mathrm{Re})^{1/2}$	$Nu_x(\mathrm{Re})^{-1/2}$	$Sh_x(Re)^{-1/2}$
0.4	0. 5	0.2	0.1	90	0.1	2.7479	0.30386	0.82017
0.6						2.9406	0.30193	0.81627
0.7						3.0374	0.301	0.81436
1.0						3.3291	0.29831	0.80878
	1					3.2317	0.29919	0.81062
	1.5					3.7207	0.29496	0.80166
	2.0					4.2133	0.29111	0.7932
		0.6				3.0069	0.30205	0.81608
		1.0				3.2667	0.30034	0.81218
		1.4				3.5273	0.29874	0.80846
			0.5			2.6866	0.2664	0.72827
			0.9			2.6854	0.25546	0.69359
			1.0			2.6853	0.25378	0.68789
				30		2.3902	0.3077	0.82774
				45		2.5089	0.30638	0.82518
				60		2.6281	0.30511	0.82265
					0.5	2.7479	0.63858	0.55933
					0.7	2.7479	0.73711	0.48089
					1	2.7479	0.84464	0.39332

4 Conclusion

In the work that is being presented here, a numerical analysis is carried out for a casson nanofluid steady-state boundary layer flow and heat transfer in a porous medium lies in an exponentially stretched surface. Velocity distribution shows a declining trend with increasing casson nanofluid parameter (β), Darcy-Forchheimer parameter Fr, porosity parameter (K_p), inclined angle (α) as well as magnetic field (M) values, but temperature and concentration profiles show a rising trend with these same parameters. The temperature profile boosts as N_t, N_b, and Le rise. The skin friction coefficient shows a significant correlation with the variables K_p, M, Fr, and α, and inversely associated with β. Growing values of K_p, M, Fr, α, and β result in a decline in the local Nusselt number. The Sherwood number drops with an increase in the values of K_p, M, Fr, β, Pr, N_b, and α, while it boosts with Le and N_b. A reduction in the momentum boundary layer thickness and inflation in the thermal boundary layer thickness is caused due to the porous medium. Conductive heat transfer dominates for increasing permeability of the medium. All these factors help in enhancement of heat and mass transfer.

References

1) Chandel S, Sood S. Unsteady flow of Williamson fluid under the impact of prescribed surface temperature (PST) and prescribed heat flux (PHF) heating conditions over a stretching surface in a porous enclosure. *ZAMM - Journal of Applied Mathematics and Mechanics / Zeitschrift für Angewandte Mathematik und Mechanik*. 2022;102(3). Available from: https://doi.org/10.1002/zamm.202100128.
2) Sharma S. Study on Darcy-Forchheimer Flow and MHD Boundary Layer Flow with Heat Transfer Characteristics of Williamson Nanofluid Over Curved Stretching Surface. *Journal of Physics: Conference Series*. 2021;1979(1):012046. Available from: https://doi.org/10.1088/1742-6596/1979/1/012046.
3) Arifuzzaman M, Uddin MJ. Convective flow of alumina–water nanofluid in a square vessel in presence of the exothermic chemical reaction and hydromagnetic field. *Results in Engineering*. 2021;10:100226–100226. Available from: https://doi.org/10.1016/j.rineng.2021.100226.
4) Uddin MJ, Rasel SK. Numerical analysis of natural convective heat transport of copper oxide-water nanofluid flow inside a quadrilateral vessel. *Heliyon*. 2019;5(5):e01757. Available from: https://doi.org/10.1016/j.heliyon.2019.e01757.
5) Irfan M, Khan M, Khan WA. Heat sink/source and chemical reaction in stagnation point flow of Maxwell nanofluid. *Applied Physics A*. 2020;126(11):1–8. Available from: https://doi.org/10.1007/s00339-020-04051-x.
6) Rafiq K, Irfan M, Khan M, Anwar MS, Khan WA. Arrhenius activation energy theory in radiative flow of Maxwell nanofluid. *Physica Scripta*. 2021;96(4):045002. Available from: https://doi.org/10.1088/1402-4896/abd903.
7) Irfan M. Study of Brownian motion and thermophoretic diffusion on non-linear mixed convection flow of Carreau nanofluid subject to variable properties. *Surfaces and Interfaces*. 2021;23:100926. Available from: https://doi.org/10.1016/j.surfin.2021.100926.
8) Darcy H. Les fontaines publiques de la ville de Dijon: exposition et application. .
9) Kumar YS, Hussain S, Raghunath K, Ali F, Guedri K, Eldin SM, et al. Numerical analysis of magneto hydrodynamics casson nanofluid flow with activation energy, Hall current and thermal radiation. *Scientific Reports*. 2023;13(1):4021. Available from: https://doi.org/10.1038/s41598-023-28379-5.
10) Waini I, Ishak A, Pop I. On the stability of the flow and heat transfer over a moving thin needle with prescribed surface heat flux. *Chinese Journal of Physics*. 2019;60:651–658. Available from: https://doi.org/10.1016/j.cjph.2019.06.008.
11) Sharma D, Sood S. Effect of inclined magnetic field on flow of Williamson nanofluid over an exponentially stretching surface in Darcy-Forchheimer model. *ZAMM - Journal of Applied Mathematics and Mechanics / Zeitschrift für Angewandte Mathematik und Mechanik*. 2022;102(6):202100425. Available from: https://doi.org/10.1002/zamm.202100425.
12) Mustafa M, Hayat T, Pop I, Aziz A. Unsteady boundary layer flow of a Casson fluid due to an impulsively started moving flat plate. *Heat Transfer—Asian Research*. 2011;40(6):563–576. Available from: http://dx.doi.org/10.1002/htj.20358.
13) Eldabe NT, Saddeck G, El-Sayed AF. Heat transfer of MHD non-Newtonian Casson fluid flow between two rotating cylinders. *Mechanics and Mechanical Engineering*. 2001;5(2):237–251.
14) Kuznetsov AV, Nield DA. Natural convective boundary-layer flow of a nanofluid past a vertical plate. *International Journal of Thermal Sciences*. 2010;49(2):243–247. Available from: https://www.infona.pl/resource/bwmeta1.element.baztech-article-LOD7-0033-0089.
15) Shampine LF, Kierzenka J, Reichelt MW. Boundary Value Problems for Ordinary Differential Equations. *SIAM Journal on Numerical Analysis*. 1968;5(2):219–242. Available from: https://classes.engineering.wustl.edu/che512/bvp_paper.pdf.
16) Magyari E, Keller B. Heat and mass transfer in the boundary layers on an exponentially stretching continuous surface. *Journal of Physics D: Applied Physics*. 1999;32(5):577–585. Available from: https://doi.org/10.1088/0022-3727/32/5/012.
17) Sharma S. MHD Boundary Layer Flow Past an Exponentially Stretching Sheet with Darcy-Forchheimer Flow of Nanofluids. *Indian Journal Of Science And Technology*. 2022;15(33):1594–1604. Available from: https://doi.org/10.17485/IJST/v15i33.607.